RESEARCH ARTICLE   OPEN ACCESS

Integrated Petrophysical Parameters and Petrographic Analysis Characterizing Khartam Reservoirs of the Permo-Triassic Khuff Formation, Saudi Arabia

K Al-Khidir(*): M Benzagouta*, A Al-Qurishi**, A Al-Laboun

College of Engineering, Al Amoudi Research Chair in Petroleum, EOR, Department of Petroleum Engineering and Natural Gas, King Saud University, Riyadh, Saudi Arabia.
Petroleum and Natural Gas Research Institute, King Abdulaziz City for Science and Technology, Riyadh, Saudi Arabia.
College of Science Department of Geology, King Saud University, Riyadh, Saudi Arabia.

ABSTRACT
Measured porosity and permeability were integrated with thin section petrography and pertophysical attributes derived from mercury intrusion to form an essential outline for Khartam reservoirs of the Permo-Triassic Khuff Formation. Porosity-permeability distribution of thirty two outcrop core samples delineates an existence of five demonstrative pertophysical facies. Thin section petrography reveals dissolution as principal diagenetic feature controlling fluid flow in Khartam reservoirs. Based on dissolution and poro – perm distribution it was found that, better khartam reservoirs quality confined to dolostone facies type (QK1) and tidat flat oolite grainstone facies (QK27) with higher degree of dissolution owing to cement removal. Further supports to dissolution statement come from physical attributes acquired from mercury intrusion including pore size distribution tail and total cumulative intrusion volume. Correspondingly facies with higher pore size distribution tail and higher total cumulative intrusion volume restricted to dolostone facies type (QK1) and oolite grainstone facies type (QK27).
Keywords: Khartam reservoirs, Khuff Formation, dissolution, cumulative intrusion volume, pore size distribution tail

I.   1.Introduction

The Permo-Triassic Khuff Formation exposed in central Saudi Arabia is bracketed between the Permo-Carboniferous Unayzah Formation at the base and Triassic Sudayr Formation at the top. The term Khuff limestone member informally introduced by Steineke ,1937, unpub. Rep., and was raised to formational status by Bramkamp et al. 1945, unpub. Rep.in Powers et al 1966 [1].The measured and described section of the Khuff limestone in the vicinity of Ar-Rayn was modified and published as a reference section for the amended Khuff Formation by Bramkamp et al. 1945, unpub. Rep., Powera etal 1966 [1]. Later, Holm et al. ,1948, unpub. Rep., measured and described Khuff limestone in Buraydah region and subdivided the formation into three members, defined from base to top as Lower Khuff limestone, Midhnab shale and Khartam limestone, in Al-laboun 1993[2].

The term Khuff first appeared in publication by Steineke and Bramkamp 1952b, [3]. Later, the same term appeared in the stratigraphic succession of Saudi Arabia rock units by Thralls and Hasson,1956, [4]. However, the formation was formally defined by Steineke et al. 1958, [5]. In 1966 Powers et al. [1] summarized the early work of Holm et al. 1948,

unpub, rep., Gierhart and Owens ,1948, unpub, rep., Pocock and Kopp ,1949, unpub, rep., Gierhart and Ramirez 1949, unpub, rep. and Henry and Bramkamp ,1950. They published a reference section of the amended Khuff Formation discarding previous nomenclature of Holm et al. 1948. They subdivided the formation into four lithologic units, listed from bottom to top as dolomite and shale, dolomite and limestone, aphanitic limestone and aphanitic-calcarintic limestone. The basal unit was deposited nonconformably on Precambrian basement complex.

The published Khuff Formation age is assigned as Permian or probably upper ,Steineke et al, 1958, [5] and/or Upper Permian ,Powers et al., 1966, [1]. This was revised by Vaslet and Fauconnier ,1982, in Al-Laboun 1993 [2].The pollens, spores, and acritarchs extracted from the Khuff Formatiom proved its age as Middle-Upper Permian age.

Laboun ,1982, [6] defined a new formation named Unayzah Formation composed of the basal siliciclastics and minor carbonates and anhydrites of the Khuff Formation. Later, Delfour et al. 1983, [7] subdivided Khuff Formation of the Ad-Dawadimi quadrangle into five informal members defined from base to top as Unayzah, Huqayl, Duhaysan, Midhnab and Khartam. They re-instated Khartam and Midhnab

members, originally introduced by Holm et al. (1948) and discarded by Powers et al. 1966, [1] The five informal members of the Khuff Formation of Delfour et al. 1983, [7] were recognized by Manivit et al. 1983, unpub. Rep. [8] in stratigraphic Drill-Hole SHD-1 (lat. 24 13 40 N., long. 45 37 30 E.) in Durma quadrangle where the upper contact between the underlying Khartam member and the overlying Sudair Shale was picked at 413 meters. Khuff formation in Ad-Dawadimi quadrangle is separated from the underlying Saq Sandstone by a regional stratigraphic unconformity. The Khuff Formation rests on the Upper and Lower members of the Saq Sandstone, in the north and south of lat. 24 47 N respectively.

Vaslet et al. 2005, [9] studied the Permian-Triassic Khuff Formation of central Saudi Arabia and subdivided the Khuff into five members, listed from oldest to youngest as Ash Shiqqah Member, Huqayl Member, Duhaysan Member, Midhnab Member and Khartam Member. They divided the Late Permian Huqayl Member into a Lower and an Upper unit and identified two units within the Khartam member, a Lower dolomite and clayey limestone, and an Upper oolitic limestone.

The term Khartam member was named for a 30 meter limestone section exposed at Khasim Khartam near al-Midhnab town (Holm et al.,1948, unpub. Rep.). Delfour et al (1983) ,[7] described a reference section in the ad-Dawadimi Quadrangle where 27.1 meter of the member is exposed.

In central Saudi Arabia the Permo-Triassic Khartam member is well defined and well exposed. It is bracketed between the shales of Midhnab member at the base and Sudayr Formation at the top. Delfour et al 1983, [7] subdivided the Khartam Member into lithologic sequences; a lower sequence composed of bioclastic lumachelle limestone followed by blue and yellow laminated dolomitic clay and ocher bioclastic dolomite, and an upper sequence beige powdery dolomite and limestone overlain by laminated silty clay and lumachelle dolomite.

The Khartam Member was originally dated as Permian (Holm et al., 1948), Late Permian (Powers, 1968; Delfour et al.,1983; Vaslet et al.,1983, Early Triassic , Manivit et al., 1984, 1985, in Al-Laboun 1933 [2]. Early Triassic age of the Khartam member was confirmed by Vaslet et al., 1985, in the al-Faydah Quadrangle [2]. However, Manivit et al. (1986) and Vaslet et al. (2004) assigned the Khartam member exposed in the Buraydah Quadrangle to be Djulfian (Late Permian)-Scythian (Early Triassic) and Changhsingian (Late Permian)-Scythian (Early Triassic), respectively [2].

Al-Khidir et al. 2011, 2013, [10] , [11], reported a caliche surface (sub-Khuff unconformity) separating cream,burrowed limestone facies of Huqayl member of the Khuff Formation from the

underlying Shajara Formation Reservoirs of the permo-carboniferous Unayzah Group at Wadi Shajara, Qusayba area, al-qasim region,saudi Arabia.

The aim of this work is to incorporate petrophysical and petrographic analyses to form a fundemental framework for Khartam reservoirs characterization and its quality assessment.

II. Subsurface Geology

Rahim et al. 2013, [12] reported that Khuff formation represents the earliest major transgressive carbonate deposited in a shallow continental shelf in eastern Saudi Arabia. These carbonates were deposited in tidal flat environments including subtidal, intertidal and supratidal (sabkha). They reported that these depositional environments include four cycles named from top to base as Khuff-A, Khuff-B, Khuff-C, and Khuff-D, each starts with a transgressive grainstone facies that makes up the Khuff reservoirs, and ends up with regressive, muddy, anhydritic facies which makes up the non-reservoir units (reservoir seals).

Raed K. Al Dukhayyil and Aus A. Al Tawil 2006, [13] reported that the Triassic Khartam sequence boundary coincides with the Permo-Triassic Boundary that overlies a reddish Paleosol. They demonstrated that the 26-meter Khartam Member is time equivalent to the Triassic Khuff B and A carbonate gas reservoirs in Ghawar subsurface. The outcrops exhibit reservoir character similar to that observed in the subsurface and tied to similar rock fabric signatures.

Meyer et al 2004, [14] studied facies distribution, sequence stratigraphic architecture, and reservoir development within the upper Khuff Formation by comparing geological architecture of two offshore Abu Dhabi fields. They reported different diagenetic overprint leading to different static and dynamic properties.

Saleh Al-Raimi and Rami Kamal 2000, [15] developed a new layering scheme for the Khuff-B , and subdivided it into five layers , sensitive to lithofacies distribution, and easily detected on compensated formation-density/compensated neutron wireline log curves and in rock core, in addition to gamma-ray signatures. They also reported that Khuff-B oolite volumetrically comprises the bulk of the Khuff-B reservoir.

III. Experimental Procedure

Thirty two block samples of the Khartam member were collected every 0.5 meter from fresh road cut of the Riyadh-Qasim Highway Fig.1 (lat. 26° 12). The lower contact of Khartam member with Midhnab member and the upper contact with overlying Sudayr Formation are well exposed at this road cut. The outcrop of the Khartam Member of the

Permo-Triassic Khuff Formation shows presence of fracture surface and oolitic bed, Fig. 2 and Fig.3.

Thin sections were prepared for Petrographic analysis to reveal Khartam reservoirs mineralogy, depositional environments and post depositional alterations (diagenetic phases). Several cylindrical samples were cored from each block and samples permeability (K) and porosity (Φ) were measured using gas permemeter and helium porosimeter respectively. Measured permeability and porosity (Fig. 4) were used to identify the pertophysical facies.

Based on porosity-permeability distribution obtained, five samples have been selected for capillary pressure measurements utilizing Mercury Intrusion Porosimeter. The output was further used to evaluate average distribution function of Burdine et al., 1950, [16] and pore size distribution (PSD). Likewise plots of cumulative intrusion volume versus capillary pressure were utilized to confirm post depositional alterations (dissolution).

IV.   Results and Interpretation
IV.I Porosity-Permeability Distribution

The porosity-permeability distribution of the cored samples is shown in Fig. 4. Using Tieb and Donaldson 2012, [17] classification of pertophysical facies, the results delineate five facies defined as

A. Good porosity, moderate permeability,
B. Good porosity, moderate fair permeability,
C. Poor porosity, fair permeability,
D. Good porosity, fair permeability,
E. Very good porosity, moderate permeability.

Facies A is represented by sample QK1, a dolostone type with appreciable dissolution Fig. 4 and 5. Facies B is represented by sample QK13 is oolitic grainstone type with lower degree of dissolution Fig. 4 and Fig. 8. Further pronounced reduction in porosity and permeability is assigned to facies C represented by sample QK16 cracterized by its fine grains reproduced by compaction Fig.4 and Fig.11. Slight increase in permeability and appreciable increase in porosity attributed to oolitic dissolution characterizes facies D represented by sample QK25 Fig. 4 and Fig. 14. As we proceed from pertophysical facies D to E, a noticeable increase in porosity and substantial rise in permeability was recognized. This can be attributed to the serious dissolution and oolitic charcterstics leading to better fluid flow capacity as noticed for sample QK27 Fig.4 and Fig.17. Overall and based on the petrophysical distribution, the best attributes consign to dolostone facies (QK1) and oolite grainstone facies (QK27).

IV.II Petrographic Analysis

The petrographic analysis conducted aimed at defining khartam reservoir mineralogy, depositional environments, in addition to diagenetic features which play an important role in storage and fluid flow capacities. Thin sections were made for all outcrop samples, but five representative samples were selected based on their porosity-permability distribution.

Fig. 5 illustrates a microphotograph of facies A represented by sample (QK1). It is described as dolostone type with a noticeable degree of dissolution represented by a light gray color and ferruginization (red color) as diagenetic phases. Fig. 8 presents a microphotograph of facies B (QK13) identified as an oolitic grainstone type representing tidal flat, high energy depositional environment. Dissolution and ferruginization are the main diagenetic features of this facies. Facies C is demonstrated in microphotograph shown in Fig. 11 for sample (QK16). It is described as fine grains limestone with localized fractured surface and a lesser degree of dissolution due to compaction. Fig. 14 shows a microphotograph of facies D recognized as porous limestone (QK25) with no pores interconnection. Fig. 17 presents a microphotograph of facies E designated as oolitic grainstone (QK27) with an extensive dissolution leading to cement removal as illustrated by the blue color. Consequently, porosity is mainly of secondary origin due to late diagenetic dissolution of the cement. Fontana et al. 2010, [18] supported the cement dissolution reporting that Khuff Formation analogues do not have significant primary porosity. Further supports to dissolution enhanced porosity come from Mazzullo and Harris ,2009, [19] who reported new porosity creation by dissolution in deep-burial, mesogenetic environment owing to the effect of fluids charged with organic acids, carbon dioxide and hydrogen sulfide generated during organic maturation in source rocks and hydrocarbon degradation. Therefore, relating thin section petrography to porosity-permeability distribution, indicate the role dissolution on permeability enhancement and hence the better Khartam reservoirs characteristics (Qk1 and QK27).

IV. III Mercury Intrusion

Mercury intrusion tests were conducted on the five selected Khartam porosity-permeability facies to reveal Khartam reservoirs pore geometry and quality confirmed by cumulative intrusion volume. Fig. 6 is the pore size distribution of facies A (QK1) described as dolostone type. The Fig. identifies a unimodal pore geometry with a tail skewed towards large pore throat radii ranging from 0.01 to 68 μm. This facies is also characterized by a total cumulative intrusion volume up to 0.20 ml as shown in Fig. 7.

Fig. 9 is the pore size distribution of facies B (QK13) identified as oolitic grainstone. This Fig. identifies a bimodal pore size distribution with a tail from 0.1 to 68 μm. In addition to that is also characterized by a total intrusion volume of 0.17 ml as recognized in Fig. 10.

Fig. 12 demonstrates a bimodal pore size distribution of facies C (QK16) with two distinctive peaks. The biggest peak posses pore throat radius equivalent to 0.009 μm, however the smallest one is around 0.06 μm. Reduction in total cumulative intrusion volume (0.025 ml) as displayed in Fig. 13 is due to its fine grains limestone characteristics regenerated by compaction.

The bimodal pore size distribution for facies D (QK25) is presented in Fig. 15. This facies is characterized by two nearly identical summits distribution in height but with different pore throat radius. The largest pore radius is about 0.007 μm , whereas the smallest one is around 0.03 μm. Facies D is also characterized by skewence ranging from 0.1 to 68 μm. This facies posses a total cumulative intrusion volume of 0.11 ml as shown in Fig. 16. As we progress from facies D to facies E (QK27) the pore size distribution is converted from bimodal to monomodal but with an essential increase in pore size distribution extension from 0.01 to 68 μm as shown in Fig. 18. This facies is characterized by a total cumulative intrusion of 0.26 ml as identified in Fig. 19. This can be attributed to the intensive dissolution of oolitic grain stone as identified from the microphotograph ,Fig.17 of that sample.

Generally, combining the mercury intrusion results with the petrographic analysis and porosity-permeability distribution indicate that, the more skewed the pore size distribution, the higher the dissolution and permeability and hence the better khartam reservoirs characteristics (QK1 and QK27). Fluid flow increase with the increase of dissolution is also confirmed by cumulative intrusion volume. That is to say, the higher the cumulative intrusion volume, the higher the dissolution, the higher the permeability, the better the Khartam reservoirs characteristics (dolostone facies and oolite grain stone facies).

V.   Conclusion
The aim of this work is to incorporate petrophysical and petrgraphic analyses to form a fundemental framework for Khartam reservoirs characterization and its quality assessment. Porosity, permeability, pore size distribution and cumulative intrusion volume constitute the pertrophysical attributes. The porosity – permeability distribution allocates existence of five illustrative petrophysical facies.   The pore size distribution of Khartam reservoirs of the Permo-Triassic Khuff Formation is characterized by mono modal to bimodal geometry

with a clear tailing towards larger pore size reflecting a heterogeneous system. Better Khartam reservoirs quality assigned to mono pore type in the pathway of dolostone facies and oolite grainstone facies type. This broadcast was also supported by mercury cumulative intrusion volume which noticeably increases in the trajectory of dolostone facies and oolite grainstone facies.

Thin section petrography reveals dissolution, fracturing, ferruginization and compaction as diagenetic features and tidal flat as depositional environment. Dissolution was found to be the principal diagenetic phase controlling Khartam reservoirs quality. That is to say, the higher degree of dissolution, higher permeability, longer the tail of pore size distribution , higher cumulative intrusion volume in the track of dolostone facies and oolite grainstone facies.

VI.   Acknowledgement

References
[1] R Powers, L Ramirez, C. Redmon and E. Elberg, *Geology of the Arabian Peninsula, sedimentary geology of Saudi Arabia. United States Geological Survey, Professional Paper, 560-D,* 1966, 147 p.

[2] A Al-Laboun, *Lexicon of the Paleozoic and Lower Mesozoic of Saudi Arabia (Part-1 : Lithostratigraphic Units,* Nomenclature Review), *Al-Hudhud Publishers,* Box 63280 Riyadh 11516, 1993.

[3] M. Steineke, and R. Bramkamp , In, W. Arkell (Ed.), *Stratigraphical introduction. Jurassic Ammonites from Jebel Tuwaiq, Central Arabia, Royal Society of London Philosophical Transactions, ser. B, v. 236,* 1952b, 241-313.

[4] H Thralls, and R. Hasson, *Geology and oil resources of eastern Saudi Arabia. 20th International Geology Congress, Mexico and Symposium sobre Yacimentos de Petrpleum and Gas, 2,* 1956, 9-32.

[5] M. Steineke, R. Bramkamp and N. Sander, *Stratigraphic relations of Arabian Jurassic oil.* In, L.G. Weeks (Ed.), *Habitat of Oil. American Association of Petroleum Geologists Symposium, 1958 ,*1294-1329.

[6] A Al-Laboun, *Subsurface stratigraphy of the Pre-Khuff formations in central and northwestern Arabia.* PhD thesis, *King Abdulaziz University, Jeddah, Kingdom of Saudi Arabia,* 1982.

[7] J Delfour, R. Dhellemmes, P. ELSASS , D. Vaslet, SE. Bros, Y-M. Nindre, and O. Dottin, *Geologic map of the Ad Dawadimi quadrangle, sheet 24G, Kingdom of Saudi Arabia .Saudi Arabian Deputy Ministry for Mineral Resources, Jeddah,Geoscience Map GM60,* 1982.

[8] J Manivit, D. Vaslet, Y.-M. Le Nindre, and F. Vaillant, *Stratigraphic drill hole SHD-1 through the lower part of the Jilh Formation, Sudair Shale and Khuff Formation in the Durma quadrangle*, sheet 24H, *Saudi Arabian Directorate General of Mineral Resources, open file report 0F-03-50,* 1983,1-34.

[9] D Vaslet, Y-M. Le Nindre, D. Vachard, J. Broutin, S. Crasquin-Soleau, M. Berthelin, J. Gaillot, M. Halawani and M. Al-Husseini, *The Permian-Triassic Khuff Formation of central Saudi Arabia. GeoArabia, Gulf PetroLink, Bahrain, 10(4),* 2005 77-134.

[10] K Al-Khidir, A. Al-Laboun, A. Al-Qurishi and M. Benzagouta, *Bimodal pore size behavior of the Shajara formation reservoirs of the Permo-Carboniferous Unayzah Group, Saudi Arabia. J Petrol Explor Prod Technol 1(1),* 2011, 1-9.

[11] K Al-Khidir, M. Benzagouta, A. Al-Qurishi, and A. Al-Laboun , *Characterization of heterogeneity of the Shajara reservoirs of the Shajara formation of the Permo-Carboniferous Unayzah group. Arab J Geosci 6 (10),* 2013, 3989–3995.

[12] Z Rahim, H. Al Anazi, A. Al-Kanaan, C. Fredd and M. Nihat Gurmen, *Evolving Khuff Formation gas well completions in Saudi Arabia: technology as a function of reservoir characteristics improves production. Saudi Aramco journal of technology* 2013.

[13] R Al Dukhayyil, and A, Al Tawil, Saudi ARAMCO, Dhahran, *Reservoir Architecture of the Triassic Khartam Carbonate Sequence*, Khuff Outcrop Analogue in Al-Qassim, central Saudi Arabia. *GEO 2006 Middle East Conference and Exhibition;* 27-29 March, 2006; Manama, Bahrain.

[14] A Meyer, R. Bochard, I. Azzam, and A. AL-Amoudi, 2004. *The upper Khuff formation, sedimentology and static core rock type approach - comparison of two offshore Abu Dhabi fields. Abu Dhabi International Conference and Exhibition,* 10-13 October 2004, Abu Dhabi, United Arab Emirates.

[15] S Al-Raimi, and R. Kamal, *A new layering scheme for the Khuff-B depositional cycle in the subsurface of eastern Saudi Arabia*, 4th Middle East Geosciences Conference, GEO 2000. *GeoArabia, Abstract, 5(1),* 2000, p. 34.

[16] N Burdine, L Gournay, and P. Reichertz, *Pore size distribution of petroleum reservoir rocks. Petrolum Transactions, AIME. Vol.189.,*1950.

[17] D Tiab, and C. Donaldson, *Petrophysics, theory and practice of measuring reservoir rock and fluid transport properties (Third Edition: Elsevier,*2012).

[18] S Fontana, F. Nader, S. Morad, A. Ceriani, and I. Al-Aasm, *Diagensis of the Khuff Formation (Permian – Triassic*, north United Arab Emirates. *Arabian Journal of Geosciences. 3(4),*2010, 351-368.

[19] S Mazzullo, and P. Harris, *An overview of dissolution porosity development in the deep-burial environment, with examples from Carbonate Reservoirs in the Permian Basin. Search and Discovery Article* #60028 , 2009.

Figure 1: The lower contact of the Khartam member with underlying Midhnab member in Al-Qasim region in central Saudi Arabia. Lat.26° 12.
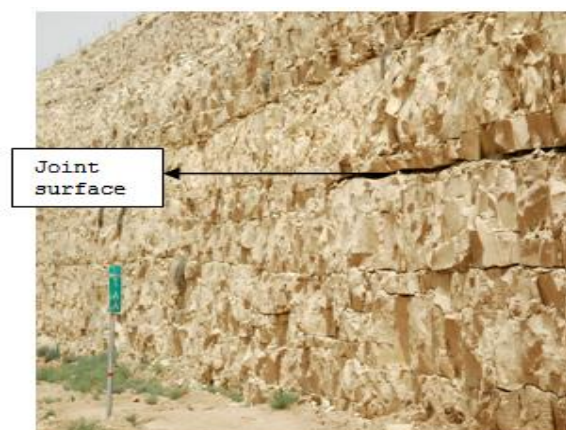

Figure 2: The Member exposed along the Riyadh al-Qasim Highway at al Khararah area, Al-Qasim region, showing presence of a fracture surface.

Figure 3: Photograph showing one of the lower oolitic beds of Khartam member exposed along the Riyadh-Al-Qasim Highway at al Khararah area, al-Qasim region in central Saudi Arabia
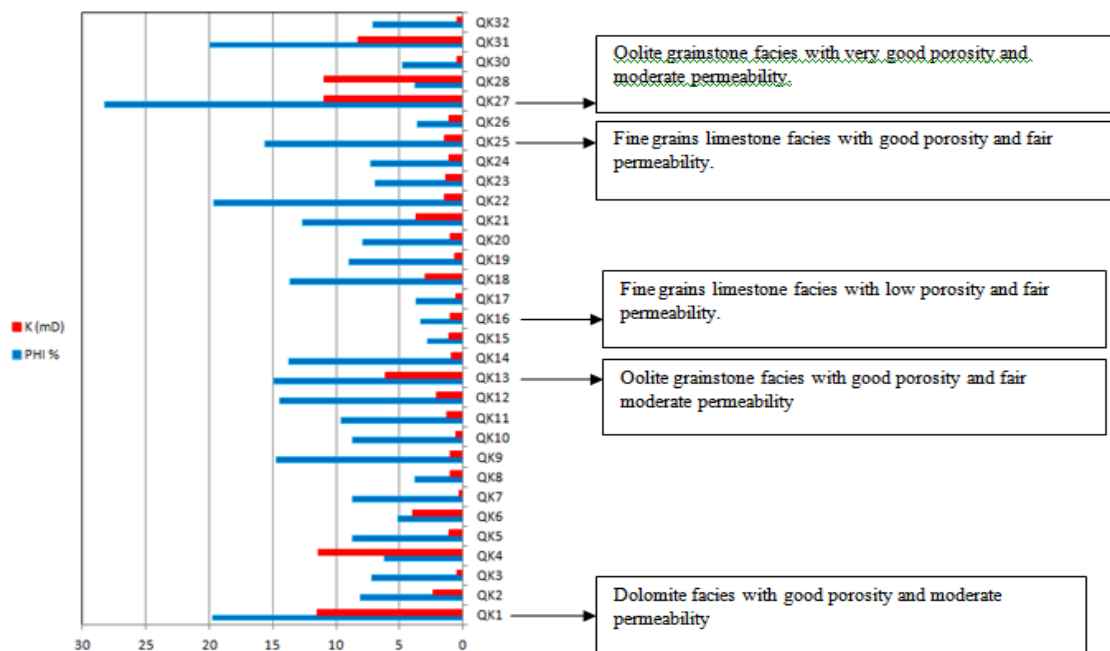

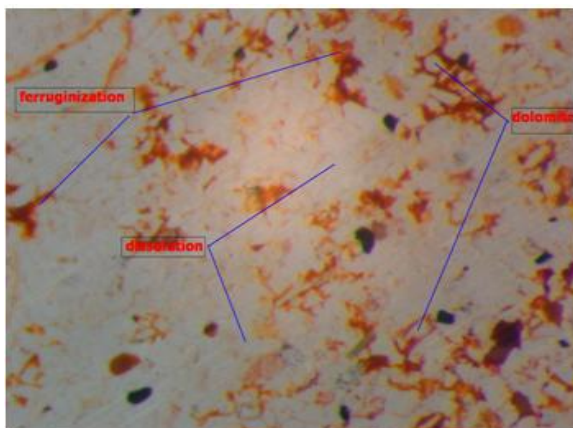Figure 4: Porosity-permeability distribution for Khartam outcrop samples

Figure 5: Microphotograph for dolostone facies QK1 showing high degree of dissolution (light gray color). Mag. 21%, Field 11 mm, Focus +0.92 mm.
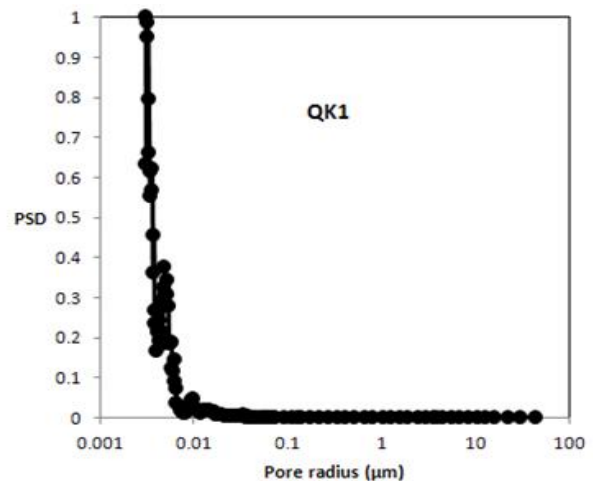

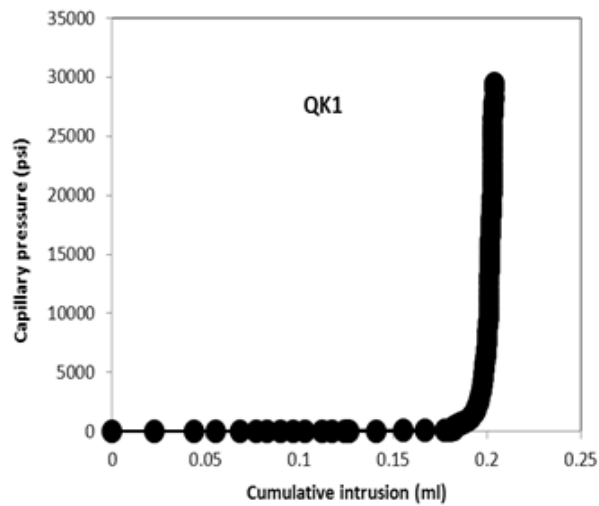Figure 6: Pore size distribution versus pore radius for sample QK1.
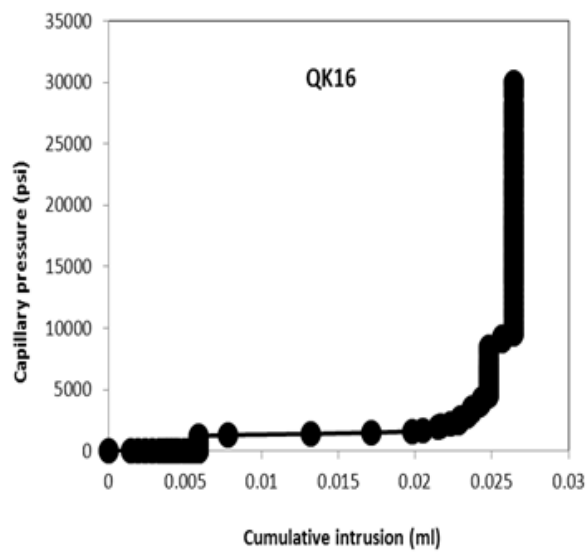
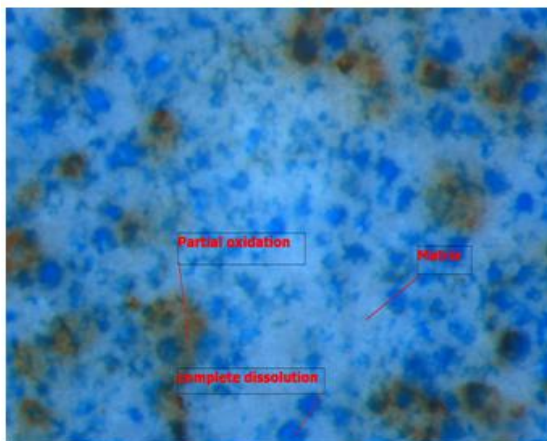Figure 7: Capillary pressure (psi) versus cumulative intrusion volume (ml) for sample QK1.
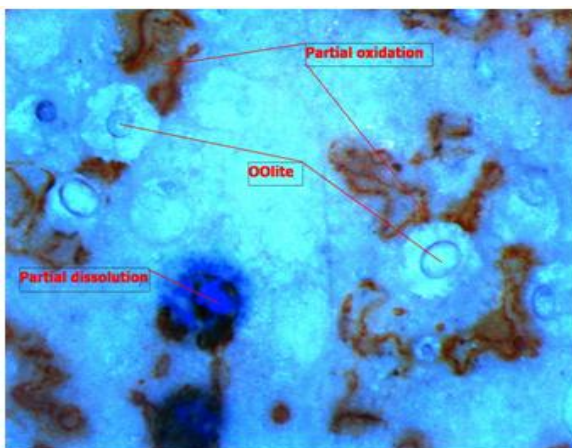
Figure 8: Microphotograph for sample QK13 showing dissolution, ferruginization, and presence of oolites indicating tidal flat depositional environment. Mag. 49.5%, Field 4.7 mm, Focus -0.08 mm.
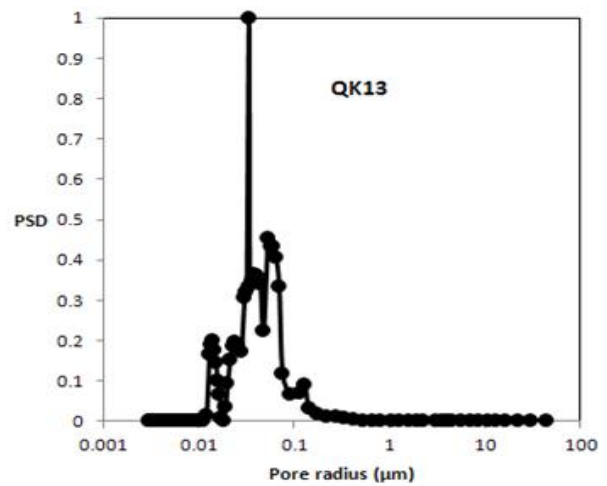
Figure 9: Pore size distribution versus pore radius for sample QK13.
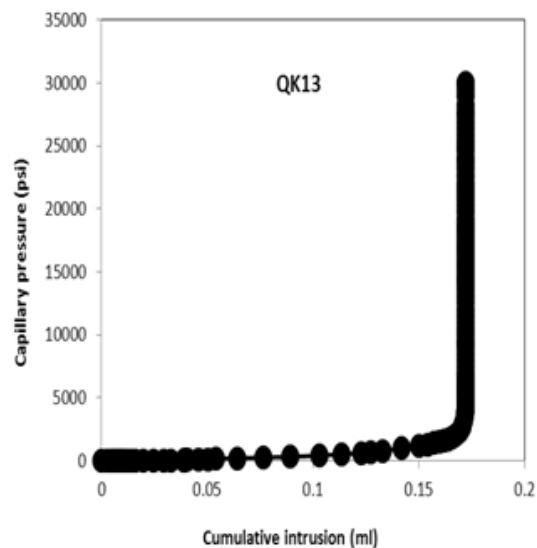
Figure 10: Capillary pressure (psi) versus cumulative intrusion volume (ml) for sample QK13.
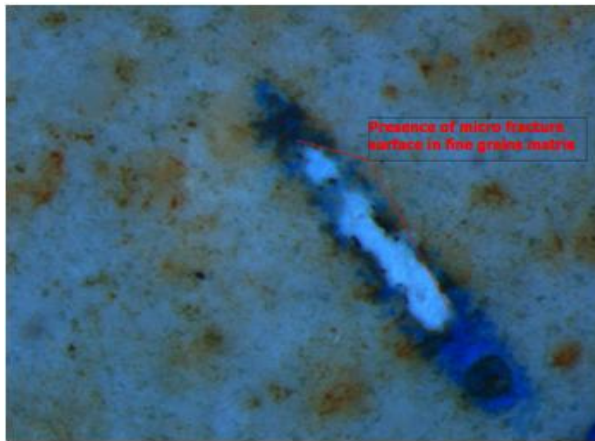
Figure 11: Microphotograph for sample QK16 displaying fine grains matrix with a fracture surface. Mag. 59%, Field 3.9 mm, Focus +0.06 mm.
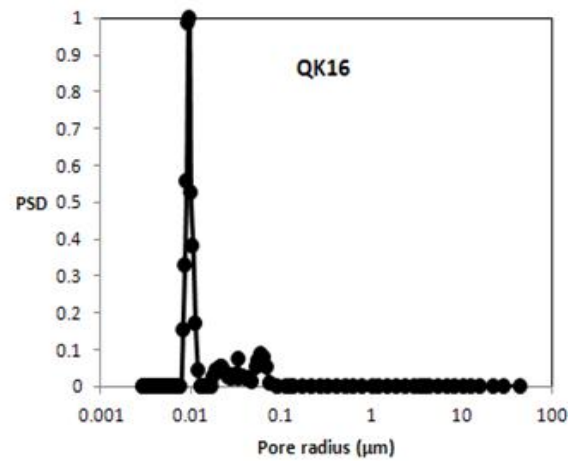
Figure 12: Pore size distribution versus pore radius for sample QK16.

Figure 13: Capillary pressure (psi) versus cumulative intrusion volume (ml) for sample QK16.

Figure 14: Microphotograph for sample QK25 with dissolution (blue color) and ferruginization (red color). Mag.100%, Field 2.3 mm, Focus -0.03 mm.
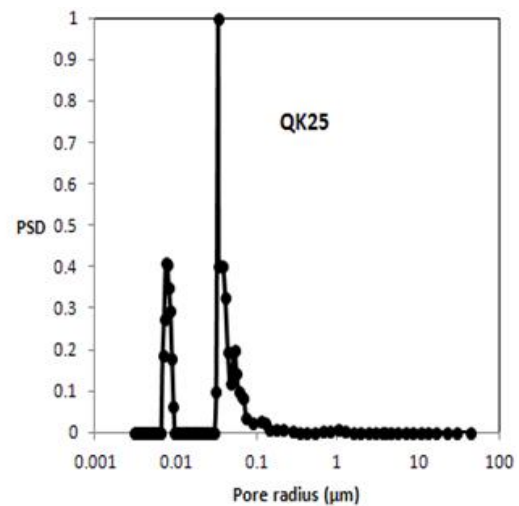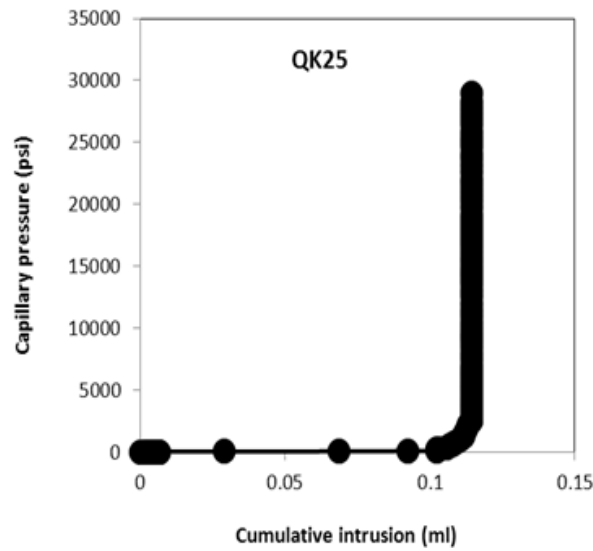

Figure 15: Pore size distribution versus pore radius for sample QK25.

Figure 16: Capillary pressure (psi) versus cumulative intrusion volume (ml) for sample QK25.
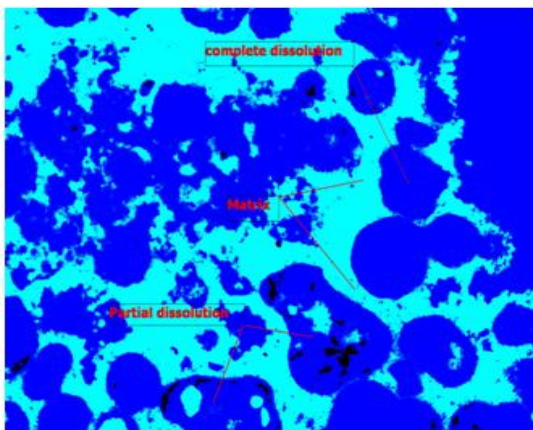

Figure 17: Microphotograph for sample QK27 assigning for intensive dissolution (blue color). Mag. 3.5 %, Field 6.5 mm, Focus +0.4 mm.
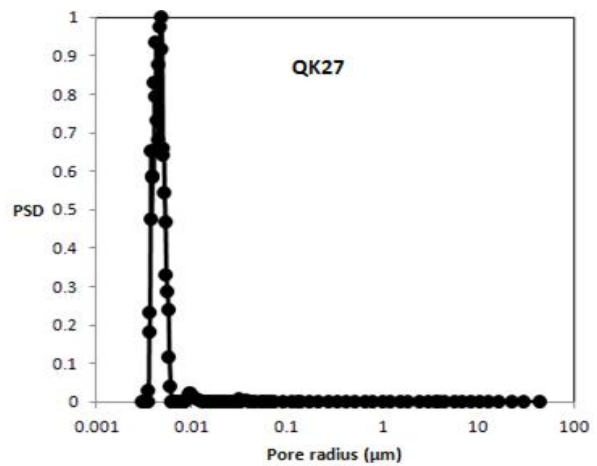

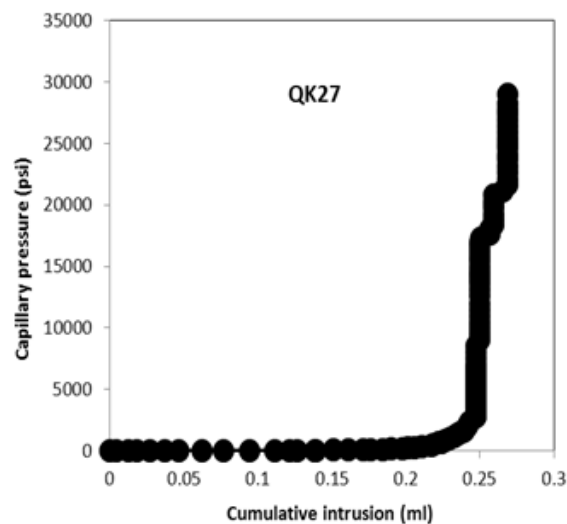Figure 18: Pore size distribution versus pore radius for sample QK27.

Figure 19: Capillary pressure (psi) versus cumulative intrusion volume (ml) for sample QK27.